Intersecting resonances and chaos in a threeoscillator model. I. Classical studies

Keith M. Atkins and David E. Logan

Citation: The Journal of Chemical Physics **97**, 2438 (1992); doi: 10.1063/1.463082
View online: http://dx.doi.org/10.1063/1.463082
View Table of Contents: http://scitation.aip.org/content/aip/journal/jcp/97/4?ver=pdfcov
Published by the AIP Publishing

Intersecting resonances and chaos in a three-oscillator model. I. Classical studies

Keith M. Atkins[a] and David E. Logan
University of Oxford, Physical Chemistry Laboratory, South Parks Road, Oxford OX1 3QZ, United Kingdom

(Received 18 February 1992; accepted 4 May 1992)

We consider a model system of three weakly coupled, weakly anharmonic oscillators, containing two near 2:1 Fermi resonances. This system is initially reduced via a resonance approximation to one of two coupled pendula, each pendulum representing one of the interoscillator resonances. This leads to a natural description of the system in terms of analytically predictable resonance zones and their intersection in action space. A full numerical analysis of the classical dynamics of the two-pendulum system is given, with respect to both the appearance of stochasticity and the development of periodic orbits in the resulting two-dimensional area-preserving map. The success of the resonance approximation in describing adequately the behavior of the three-oscillator model is shown by comparison with a representative study of the classical dynamics of the full three-oscillator model.

I. INTRODUCTION

The problem of intramolecular energy redistribution has long provoked study of the classical and quantum dynamics of simple systems of coupled oscillators.[1–8] Particular attention has been given to models of two-coupled oscillators, of which the Hénion–Heiles or Barbanis systems provide simple examples, although much attention has also been given to more realistic examples in the context of chemical dynamics.[9] For such, it is generally found that at low energies the classical dynamics are regular, and that a transition to chaotic behavior occurs as energy is increased. Since the transition to chaos involves a single oscillator pair, it typically occurs in a relatively strong interoscillator coupling regime at energies fairly close to the dissociation threshold.

In higher-dimensional systems, and for real polyatomic molecules in particular, facile energy flow may alternatively be induced in a weak-coupling regime via *intersection* of the lowest-order Fermi resonances associated with *distinct* oscillator combinations (see, e.g., Refs. 10 and 11), in contrast to a resonance overlap route to chaos relevant to a single oscillator pair. Classically chaotic dynamics may thus result in an energy range well below any dissociation threshold, where the individual oscillators may reasonably be regarded as weakly anharmonic, and the role of higher-order resonances is likely to be of secondary importance.

For conservative systems, a given primary resonance involves at least one pair of oscillators. To realize the possibility of such a resonance intersecting another which does not involve the same combination of oscillators, one requires at minimum an $N=3$ degree-of-freedom system. Since, for $N>3$ degree-of-freedom systems, facile energy flow may involve the successive participation of distinct Fermi resonances,[10–12] it is clearly important to understand the basic structure and consequent dynamics of a single intersecting resonance pair. This we aim to consider with reference to a simple three-oscillator model, the classical dynamics of which are investigated in the present work, and whose corresponding quantum-mechanical behavior will be described in a subsequent paper;[13] some preliminary results have recently been given.[14]

The model Hamiltonian is described in Sec. II. It contains the basic elements necessary to study an interacting pair of distinct primary resonances (and, as discussed in Refs. 13 and 14, has the virtue of being readily quantized). Nonlinearity is introduced into the individual oscillators as a simple function of their actions alone; the harmonic frequencies are chosen such that there exist two near 2:1 Fermi resonances involving different ocillator pairs; and interoscillator energy flow, with the consequent possibility of chaos, is induced via direct coupling across the directions of the two primary resonances. The Hamiltonian is reduced to an appropriate dimensionless form, and the model parameters used in this work are specified.

In Sec. III we first perform a canonical transformation of the Hamiltonian in order to emphasize the "slow-moving" angle terms primarily responsible for energy flow across the resonances. A resonance approximation,[1,15] whereby fast-moving angle terms are averaged over, is then invoked. This in effect reduces the full three-degree-of-freedom system to a two-degree-of-freedom one, and the resulting resonance Hamiltonian is in essence that for two-coupled pendula. Each pendulum essentially corresponds to a resonance between one pair of oscillators, and the coupling of the pendula reflects an interaction between the two resonances which arise from distinct oscillator pairs; clearly the two-degree-of-freedom resonance Hamiltonian is generically different from two-degree-of-freedom coupled oscillator systems. The location in action space of the line of resonance centers for resonances between a given oscillator pair is then discussed, together with estimates for the associated resonance widths. Three relevant domains of action space are

[a] Current address: Baker Laboratory, Department of Chemistry, Cornell University, Ithaca, NY 14853.

 0021-9606/92/162438-13$06.00

thereby identified: one which lies outside the resonance zones for either interoscillator resonance, regions corresponding to the resonance zone for a single interoscillator resonance, and the *intersection zone* where the resonance zones for the two interoscillator resonances intersect.

It is in the intersection zone that we would anticipate the possibility of widespread chaos. This is investigated in Sec. IV for the two-pendulum Hamiltonian stemming from the resonance approximation (a nonlinear mechanical system of interest in its own right). The method of Poincaré sectioning is used. It is indeed found that the most widespread chaos is associated with the intersection zone region, with predominately regular dynamics at lower and higher energies; and the physical interpretation of phase-space structures in the relevant energy domains is discussed.

In Sec. V we study, by a stability matrix method, the evolution of representative fixed points and periodic orbits of the two-pendulum system as the single parameter, energy, is varied in the two-dimensional area-preserving map. In particular, characteristic features common to a wide range of area-preserving maps are described.

To examine the extent to which the resonance approximation is adequate, we describe in Sec. VI results from a classical study of the full three-oscillator system, with particular emphasis on regions of the six-dimensional phase space associated with the resonance and intersection zones of the two-pendulum system. The principal method used is that of Lyapunov exponents. The resonance approximation appears to be a good one; the extent of the resonance zones in the three-oscillator system seem well described by the results of Sec. III; and the most widespread chaos is indeed found to be associated with the intersection zone region. Brief consideration is also given to possible Arnol'd diffusion[1] in the three-oscillator system, for which evidence is not found.

II. THE HAMILTONIAN

In this paper, the model Hamiltonian for an individual anharmonic oscillator i is taken to be

$$H_0(J_i) = \overline{\omega}_i J_i + \hat{\omega}_i J_i^2, \tag{2.1}$$

where J_i is the action coordinate of the oscillator, $\overline{\omega}_i$ its fundamental (harmonic) frequency, and $\hat{\omega}_i$ the anharmonicity constant. Since $H_0(J_i)$ is independent of the conjugate angle θ_i, the action is a trivial integral of the motion, and the frequency of the oscillator is given by

$$\omega_i(J_i) = \frac{d\theta_i}{dt} = \frac{\partial H_0(J_i)}{\partial J_i} = \overline{\omega}_i + 2\hat{\omega}_i J_i. \tag{2.2}$$

This constitutes perhaps the simplest model of a nonlinear oscillator, and we employ it in part for this reason. In addition, however, we note (as discussed in Ref. 14) that the introduction of nonlinearity as a function solely of the action permits facile quantization of the oscillator Hamiltonian, and with $\hat{\omega}_i < 0$—as used in this work—the action dependence of the frequency parallels precisely that of a Morse oscillator [even though the Hamiltonian (2.1) is nondissociative].

The zeroth-order (uncoupled) Hamiltonian for the three-oscillator system we consider is thus

$$H_0 = \sum_{i=1}^{3} H_0(J_i). \tag{2.3}$$

We choose the $\{\overline{\omega}_i\}$ such that

$$2\overline{\omega}_2 \simeq \overline{\omega}_1 \simeq 2\overline{\omega}_3, \tag{2.4}$$

i.e., we have near 2:1 Fermi resonances between oscillators 1 and 2 and between oscillators 1 and 3; and the location in **J** space of the corresponding exact Fermi resonances is obtained from $\omega_1(J_1) = 2\omega_k(J_k)$, $k = 2,3$. Given the simple action dependence of the frequencies (2.2) each such resonance defines a plane in **J** space, and intersection of the planes corresponds to intersection of the two 2:1 resonances.

To induce energy flow between the oscillators, with the consequent possibility of chaotic behavior, we couple them in the direction of the above primary resonances via

$$V = \phi_2 q_1 q_2^2 + \phi_3 q_1 q_3^2. \tag{2.5}$$

q_i is the position coordinate of oscillator i, and can be expressed in terms of the action-angle coordinates J_i, θ_i via the standard transformation [Ref. (15) and Eq. (2.6) below]. For clarity, we have chosen not to couple in the direction of the near 1:1 resonance between oscillators 2 and 3. The full Hamiltonian we consider is thus $H = H_0 + V$. Further, as discussed in more detail below and in the following sections, the $\{\hat{\omega}_i\}$ are chosen such that for all J_i of interest $|\hat{\omega}_i| J_i \ll \overline{\omega}_i$, so that the dynamics of the system are dominated by the two primary 2:1 Fermi resonances.

In order to work with suitably reduced parameters and coordinates, we consider the dimensionless Hamiltonian $H' = H/(\overline{\omega}_1 J_0)$ where J_0 is some scale of action. With $J_i' = J_i/J_0$, $\theta_i' = \theta_i$ and the transformations

$$\overline{\omega}_i' = \frac{\overline{\omega}_i}{\overline{\omega}_1}, \quad \hat{\omega}_i' = \frac{\hat{\omega}_i J_0}{\overline{\omega}_1}, \quad \phi_k' = \frac{\phi_k J_0^{1/2}}{\overline{\omega}_1^{5/2} m_1^{1/2} m_k},$$
$$q_i' = \left[\frac{2(J_i/J_0)}{(\overline{\omega}_i/\overline{\omega}_1)}\right]^{1/2} \cos\theta_i = \left(\frac{2J_i'}{\overline{\omega}_i'}\right)^{1/2} \cos\theta_i' \tag{2.6}$$

(where m_i is the reduced mass of oscillator i) we obtain the reduced form

$$H' = \sum_{i=1}^{3} (\overline{\omega}_i' J_i' + \hat{\omega}_i' J_i'^2) + \phi_2' q_1' q_2'^2 + \phi_3' q_1' q_3'^2 \tag{2.7}$$

with dimensionless coordinates and parameters. The measure of time is also scaled such that $t' = \overline{\omega}_1 t$, but otherwise the dynamics of H' and H are identical. In what follows we thus consider the reduced Hamiltonian but drop the prime notation.

The dimensionless parameters $\{\overline{\omega}_i, \hat{\omega}_i, \phi_k\}$ used in this work are given in Table I. There are four natural sets of energy scales in the problem: harmonic energy scales ($\sim \overline{\omega}_i J_i$), energy scales associated with differences in fundamental frequencies ($\sim \Delta\overline{\omega}_k J_i$ where $\Delta\overline{\omega}_k = \overline{\omega}_1 - 2\overline{\omega}_k$, $k = 2,3$); intraoscillator anharmonicity energy scales ($\sim \hat{\omega}_i J_i^2$), and energy scales associated with the interoscillator couplings [$\sim \phi_k (J_1 J_k^2/\overline{\omega}_1 \overline{\omega}_k^2)^{1/2}$]. The model parameters, and the total energy (and hence region of **J** space) considered in the following sections, are chosen to parallel the behavior of real weakly anharmonic molecular systems in which facile energy flow due to intersection of primary

TABLE I. The parameters used for the three-oscillator Hamiltonian.

Parameter	Value
$\overline{\omega}_1$	1.000 000
$\overline{\omega}_2$	0.498 750
$\overline{\omega}_3$	0.501 125
$\hat{\omega}_1$	−0.001 000
$\hat{\omega}_2$	−0.000 250
$\hat{\omega}_3$	−0.000 125
ϕ_2	−0.000 1
ϕ_3	−0.000 1

resonances can occur in a weak-coupling regime: the harmonic energies are thus in excess of the remaining energy scales (which have comparable magnitudes) by 2–3 orders of magnitude.

III. THE RESONANCE APPROXIMATION

In this section we first perform a canonical transformation of the Hamiltonian. The position coordinates $\{q_i\}$ appearing in the interoscillator coupling V may be written in terms of $\{J_i,\theta_i\}$ action-angle coordinates via the standard transformation.[15] This leads to $H\equiv H(\{J_i,\theta_i\})$ in the form

$$H=\sum_{i=1}^{3}\{\overline{\omega}_i J_i+\hat{\omega}_i J_i^2\}+\phi_2\left(\frac{J_1J_2^2}{2\overline{\omega}_1\overline{\omega}_2^2}\right)^{1/2}\times[2\cos\theta_1+\cos(\theta_1+2\theta_2)+\cos(\theta_1-2\theta_2)]+\phi_3\left(\frac{J_1J_3^2}{2\overline{\omega}_1\overline{\omega}_3^2}\right)^{1/2}\times[2\cos\theta_1+\cos(\theta_1+2\theta_3)+\cos(\theta_1-2\theta_3)]. \tag{3.1}$$

Because the fundamental (harmonic) frequencies are chosen such that $2\overline{\omega}_2\simeq\overline{\omega}_1\simeq 2\overline{\omega}_3$, it is clear that the $\theta_1-2\theta_2$ and $\theta_1-2\theta_3$ terms will be slow moving compared to the other angle terms in H. We thus canonically transform to a set of variables in which the slow-moving terms are emphasized, and so make the substitutions:

$$\psi_1=\theta_1-2\theta_2,\quad \psi_2=\theta_1-2\theta_3. \tag{3.2a}$$

To render the transformation canonical, it is necessary to introduce a third angle coordinate in the form

$$\psi_3=\alpha\theta_1+\beta\theta_2+\gamma\theta_3 \tag{3.2b}$$

(where α, β, and γ are constants) and produce a generating function F. We choose to write F in terms of the old angle coordinates $\{\theta_i\}$ and the new actions $\{I_i\}$, as

$$F(\{I_i,\theta_i\})=(\theta_1-2\theta_2)I_1+(\theta_1-2\theta_3)I_2+(\alpha\theta_1+\beta\theta_2+\gamma\theta_3)I_3+\theta_1J_1^r+\theta_2J_2^r+\theta_3J_3^r, \tag{3.3}$$

where the $\{J_i^r\}$ are constants to be fixed below. The choice of Eq. (3.3) for F allows considerable freedom in later simplification of the Hamiltonian to a physically transparent form, and the $J_i=\partial F/\partial\theta_i$ are given in terms of the new actions $\{I_i\}$ by

$$\begin{aligned}J_1&=I_1+I_2+\alpha I_3+J_1^r,\\ J_2&=-2I_1+\beta I_3+J_2^r,\\ J_3&=-2I_2+\gamma I_3+J_3^r.\end{aligned} \tag{3.4}$$

The Hamiltonian in terms of the new coordinates is then given by

$$H=[(\overline{\omega}_1+2\hat{\omega}_1J_1^r)-2(\overline{\omega}_2+2\hat{\omega}_2J_2^r)]I_1+(\hat{\omega}_1+4\hat{\omega}_2)I_1^2+[(\overline{\omega}_1+2\hat{\omega}_1J_1^r)-2(\overline{\omega}_3+2\hat{\omega}_3J_3^r)]I_2+(\overline{\omega}_1+4\hat{\omega}_3)I_2^2+[\alpha(\overline{\omega}_1+2\hat{\omega}_1J_1^r)+\beta(\overline{\omega}_2+2\hat{\omega}_2J_2^r)+\gamma(\overline{\omega}_3+2\hat{\omega}_3J_3^r)]I_3+(\alpha^2\hat{\omega}_1+\beta^2\hat{\omega}_2+\gamma^2\hat{\omega}_3)I_3^2+2\hat{\omega}_1I_1I_2+(2\alpha\hat{\omega}_1-4\beta\hat{\omega}_2)I_1I_3+(2\alpha\hat{\omega}_1-4\gamma\hat{\omega}_3)I_2I_3+\text{terms in the }\{J_i^r\}\text{ and the interoscillator couplings.} \tag{3.5}$$

Thus far the derivation has been general, with α, β, γ, and the $\{J_i^r\}$ arbitrary constants. We now choose the $\{J_i^r\}$ to satisfy

$$(\overline{\omega}_1+2\hat{\omega}_1J_1^r)=2(\overline{\omega}_2+2\hat{\omega}_2J_2^r)=2(\overline{\omega}_3+2\hat{\omega}_3J_3^r), \tag{3.6}$$

which elimintes terms in H which are linear in I_1 and I_2; and we choose α, β, and γ to satisfy

$$2\alpha\hat{\omega}_1-4\beta\hat{\omega}_2=0=2\alpha\hat{\omega}_1-4\gamma\hat{\omega}_3, \tag{3.7}$$

which eliminates terms bilinear in I_1I_3 and I_2I_3. The resultant Hamiltonian thus takes the form

$$H=\tfrac{1}{2}\omega_\alpha I_1^2+\tfrac{1}{2}\omega_\beta I_2^2+\omega_{\alpha\beta}I_1I_2+\text{interoscillator coupling terms}+(\text{terms in }I_3\text{ and }\{J_i^r\}\text{ only}), \tag{3.8}$$

where

$$\omega_\alpha=2(\hat{\omega}_1+4\hat{\omega}_2),\quad \omega_\beta=2(\hat{\omega}_1+4\hat{\omega}_3) \tag{3.9a}$$

and

$$\omega_{\alpha\beta}=2\hat{\omega}_1. \tag{3.9b}$$

The interoscillator couplings give rise to Fourier terms

$$\phi_kq_1q_k^2=\phi_k\left(\frac{J_1J_k^2}{2\overline{\omega}_1\overline{\omega}_k^2}\right)^{1/2}\times[2\cos\theta_1+\cos(\theta_1+2\theta_k)+\cos(\theta_1-2\theta_k)] \tag{3.10}$$

with $k=2,3$. It is however, usually argued[1,15] that only the slow-moving $\theta_1-2\theta_2$ ($\equiv\psi_1$) and $\theta_1-2\theta_3$ ($\equiv\psi_2$) combinations will have a significant effect upon the long-time dy-

namics, and so we average over (and thereby eliminate) the remaining fast-moving angle terms in the usual fashion.[1,15] This constitutes a resonance approximation, and reduces the Hamiltonian to

$$H = \tfrac{1}{2}\omega_\alpha I_1^2 + \tfrac{1}{2}\omega_\beta I_2^2 + \omega_{\alpha\beta} I_1 I_2 + V_\alpha \cos\psi_1 + V_\beta \cos\psi_2 + [\text{(cons) terms in } I_3 \text{ and } \{J_i^r\}]. \quad (3.11)$$

Here, V_α and V_β are given via Eq. (3.10) by

$$V_\alpha = \phi_2\left(\frac{J_1 J_2^2}{2\bar{\omega}_1\bar{\omega}_2^2}\right)^{1/2}, \quad V_\beta = \phi_3\left(\frac{J_1 J_3^2}{2\bar{\omega}_1\bar{\omega}_3^2}\right)^{1/2} \quad (3.12)$$

and from Eq. (3.4), depend solely on $\{I_i\}$.

The approximate Hamiltonian (3.11) is independent of ψ_3, so from Hamilton's equations $dI_3/dt = -\partial H/\partial\psi_3 = 0$ and I_3 is thus an integral of the motion: the resonance approximation in effect reduces the full three-degree-of-freedom system to a two-degree-of-freedom one. Further, from Eq. (3.4), the inverse of the canonical transformation gives I_3 as

$$I_3 = \frac{1}{2\alpha+\beta+\gamma}[2(J_1 - J_1^r) + (J_2 - J_2^r) + (J_3 + J_3^r)], \quad (3.13)$$

and so constant I_3 implies

$$J_{\text{tot}} = 2J_1 + J_2 + J_3 = \text{const}. \quad (3.14)$$

This restricts the motion to a plane in **J** space which, with $J_i \geq 0$ for all i, is a triangular section delimited by the planes $J_1 = 0, J_2 = 0, J_3 = 0$. The $J_{\text{tot}} = \text{const}$ triangle is illustrated in Fig. 1 as a projection onto the (J_2,J_3) plane, and is discused in detail below.

In determining the location of the centers of the resonances between the oscillators, the interoscillator coupling is usually assumed[1] of little significance (as is verfied numerically in Sec. VI). The resonance centers thus occur in **J** space where the conditions $\omega_1(J_1) = 2\omega_k(J_k)$ $(k = 2,3)$ are met, i.e.,

$$\bar{\omega}_1 + 2\hat{\omega}_1 J_1 = 2(\bar{\omega}_k + 2\hat{\omega}_k J_k), \quad k = 2,3. \quad (3.15)$$

Each of these conditions defines a plane in **J** space, and if the plane intersects a given $J_{\text{tot}} = \text{const}$ triangle it will do so along a line, which we refer to as the "line of resonance centers" (LORC's) for resonances between oscillator 1 and oscillator k. The two LORC's are illustrated in Fig. 1 where, for maximum illustration, the model parameters (Table I) and the value of J_{tot} $(= 44)$ have been chosen such that both LORC's lie on the $J_{\text{tot}} = \text{const}$ triangle, and also intersect each other on the triangle.

Further, the physical signficance of the constants $\{J_i^r\}$ [Eq. (3.6)] can now be made clear. From Eqs. (3.15) and (3.6) alone, the $\{J_i^r\}$ define a line in **J** space corresponding to the intersection of the two planes on which the conditions (3.15) are satisfied. If now $J_{\text{tot}}^r \equiv 2J_1^r + J_2^r + J_3^r$ is chosen to be equal to the given J_{tot}, then the $\{J_i^r\}$ are uniquely specified, and correspond to the point in **J** space at which the two LORC's intersect on the $J_{\text{tot}} = \text{const}$ plane. This is illustrated in Fig. 1, where intersection occurs on the the $J_{\text{tot}} = \text{const}$ triangle, $\mathbf{J}^r$ thus being simultaneously at the center of a resonance between oscillators 1 and 2 and at the center of a resonance between oscillators 1 and 3. In addition, since Eq. (3.13) is simply $I_3 = (J_{\text{tot}} - J_{\text{tot}}^r)/(2\alpha+\beta+\gamma)$, the choice $J_{\text{tot}}^r = J_{\text{tot}}$ corresponds to choosing $I_3 = 0$.

We now consider the widths of the interoscillator resonances, dealing explicitly with the widths of the resonances between oscillators 1 and 2 (the corresponding argument for oscillator-1–oscillator-3 resonances proceeds similarly). We thus return to Eq. (3.11) and switch off the coupling between oscillators 1 and 3, $\phi_3 = 0$, so $V_\beta = 0$. Since the resultant Hamiltonian is independent of ψ_2, it follows from Hamilton's equations that $I_2 = I_2^0$, a constant. Expanding the Hamiltonian about I_1^0 defined by $I_1^0 = -(\omega_{\alpha\beta}/\omega_\alpha)I_2^0$, and dropping constant terms, leads to a Hamiltonian describing the resonances between oscillators 1 and 2,

$$H_{\text{res}}^{12} = \tfrac{1}{2}\omega_\alpha \Delta I_1^2 + V_\alpha \cos\psi_1, \quad (3.16)$$

where $\Delta I_1 = I_1 - I_1^0$.

The physical meaning of the expansion about I_1^0 is particularly clear in **J** space, for if we invert the canonical transformation (3.4) and impose $J_{\text{tot}} = \text{const}$, we find $I_2^0 = -(1/2)(J_3 - J_3^r)$ (from which I_1^0 directly follows); and with $\phi_3 = 0$, J_3 is a trivial constant of the motion. The values (J_1^0, J_2^0) of (J_1,J_2) corresponding to I_1^0 and I_2^0 above are readily shown via Eqs. (3.4) and (3.15) to satisfy $\omega_1(J_1^0) = 2\omega_2(J_2^0)$ for the chosen J_3 on the $J_{\text{tot}} = \text{const}$ triangle. Expanding the Hamiltonian about I_1^0 thus corresponds to an expansion about the center of the oscillator-1–oscillator-2 resonance appropriate to the chosen J_3, i.e., about the point on the $J_{\text{tot}} = \text{const}$ triangle at which the LORC for oscillators 1 and 2 is intersected by the chosen constant J_3 line, as illustrated in Fig. 1. We now use Eq. (3.16) to estimate a width for an oscillator 1–2 resonance.

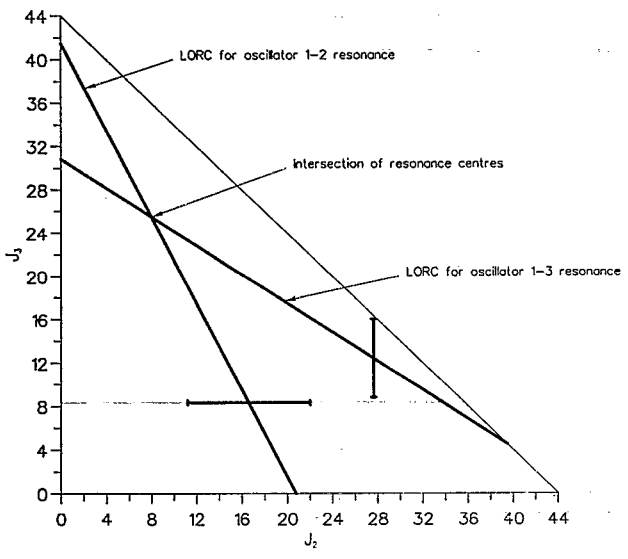

FIG. 1. The constant J_{tot} $(= 44)$ action space triangle to which motion is confined within the resonance approximation, illustrated as a projection onto the (J_2,J_3) plane. The location of the lines of resonance centers (LORC's) are shown, as are representative widths estimated as in the text. The parameters used here (and also in Figs. 2, 8, and 9) are given in Table I.

To this end we adopt the customary approximation[1,15] of constant V_α in Eq. (3.16), choosing [see Eq. (3.12)] $V_\alpha = V_\alpha(J_1^0, J_2^0)$, the specific constant value of which will depend upon the chosen value of J_3 on the given $J_{\text{tot}} = \text{const}$ triangle (so that the oscillator-1–oscillator-2 resonance width depends on J_3). Since the second term in Eq. (3.16) can move between $\pm V_\alpha$, a total range of $2V_\alpha$, the first term may also vary by this amount. This delimits the width of the resonance, as it imposes the restriction $\Delta I_1 \leqslant 2(V_\alpha/\omega_\alpha)^{1/2}$ or, equivalently, from Eq. (3.4), $\Delta J_2 \leqslant 4(V_\alpha/\omega_\alpha)^{1/2}$, leading to an estimate for the width of the oscillator 1–2 resonance at a particular value of J_3 as

$$\Delta J_{2r} = 4(V_\alpha/\omega_\alpha)^{1/2}, \tag{3.17a}$$

illustrated in Fig. 1. Similarly, for the width of the oscillator 1–3 resonance we find

$$\Delta J_{3r} = 4(V_\beta/\omega_\beta)^{1/2} \tag{3.17b}$$

with the specific value of the constant V_β dependent on the chosen value of J_2 on the $J_{\text{tot}} = \text{const}$ triangle, as also illustrated in Fig. 1.

The above analysis gives a means of estimating the location of the resonance centers and the resonance widths. The situation is summarized in Fig. 2 which shows the $J_{\text{tot}} = 44$ triangle of Fig. 1 with the LORC's and associated resonance widths as determined above, and for the model parameters of Table I used in this work. The resonance zones for resonances between oscillators 1 and 2 are indicated by horizontal lines, and the corresponding resonance zones for oscillators 1 and 3 by vertical lines. The intersection of the resonance zones is indicated by hatched lines. It is in this region that we expect the *intersection* of resonances to lead to stoachasticity. This is investigated in the following section in relation to a two-pendulum Hamiltonian, and in Sec. VI in respect to the full three-degree-of-freedom system.

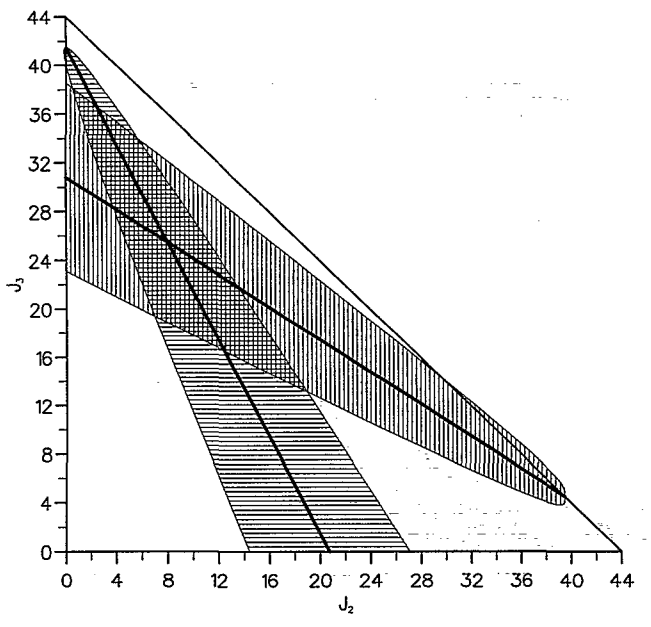

FIG. 2. The location of the LORC's and resonance zones in the $J_{\text{tot}} = 44$ triangle. Horizontal shading illustrates the resonance zone for the resonance between oscillators one and two, and vertical shading illustrates the resonance zone for the resonance between oscillators one and three. The resonance intersection zone is hatched.

IV. THE TWO-PENDULUM HAMILTONIAN

In this section we formulate and study in detail a two-pendulum approximation to the system of three-coupled oscillators. The resonance approximation described above reduces the full three-degree-of-freedom Hamiltonian to the two-degree-of-freedom resonance Hamiltonian, Eq. (3.11), motion corresponding to which is confined to a $J_{\text{tot}} = \text{const}$ triangle; in this work we choose $J_{\text{tot}} = 44$. In Eq. (3.11), the V terms arising from the interoscillator couplings depend strictly on the $\{J_i\}$ (or equivalently on I_1, I_2). To study the system numerically, however, we make one further approximation to the resonance Hamiltonian, the veracity of which is commented on in Sec. VI: V_α and V_β [Eq. (3.12)] are kept constant, the J_i's therein being assigned values $\{J_i^r\}$ corresponding to the intersection of the LORC's of Fig. 2 as discussed in Sec. III. the system we study in this section is thus specified by the Hamiltonian

$$H = \tfrac{1}{2}\omega_\alpha I_1^2 + \tfrac{1}{2}\omega_\beta I_2^2 + \omega_{\alpha\beta} I_1 I_2 + V_\alpha \cos\psi_1 + V_\beta \cos\psi_2 \tag{4.1}$$

with the V's constant as above. Although many two-degree-of-freedom systems have been studied, we are unaware of previous work on a model Hamiltonian of this form.

The model parameters $\{\bar{\omega}_i, \hat{\omega}_i, \phi_i\}$ for the three-oscillator system which are used in this work have been given in Table I. With these, and $J_{\text{tot}} = 44$, the parameters $\{\omega_\alpha, \omega_\beta, \omega_{\alpha\beta}, V_\alpha, V_\beta\}$ appearing in Eq. (4.1) are specified, and each is negative. It is of course straightforward to study the equations of motion corresponding to Eq. (4.1) with these parameter values, but as shown in the Appendix the dynamics corresponding to the Hamiltonian (4.1) are invariant to a change of sign in each of these parameters, and in practice we choose to study Eq. (4.1) with the positive parameter set. This may superficially appear to be inconvenient, but the reason is a physical one: with positive parameters, the model Hamiltonian (4.1) is that for a system of two pendula coupled via their angular momenta, a feature which permits a ready physical visualization of the resultant dynamics.

The action space triangle illustrated in Fig. 2 is a plane of constant total action, J_{tot}. It is not of course a plane of constant total energy. To illustrate this we consider the zero-order energy profile on the $J_{\text{tot}} = 44$ triangle, where the interoscillator couplings are neglected [and corresponding in the two-pendulum Hamiltonian (4.1) to neglect of the potential terms in ψ_1 and ψ_2 and retention solely of the kinetic terms]. With the parameters of Table I the zero-order energy maximum corresponds to the intersection of the LORC's on the J_{tot} triangle of Fig. 2; and the energy decreases quadratically away from this point. By inverting the signs of ω_α, ω_β, and $\omega_{\alpha\beta}$ in studying the two-pendulum system, the energy profile is simply inverted, intersection of the LORC's now corresponding to the zero-order energy miminum. The corresponding zero-order energy profile is shown in Fig. 3,

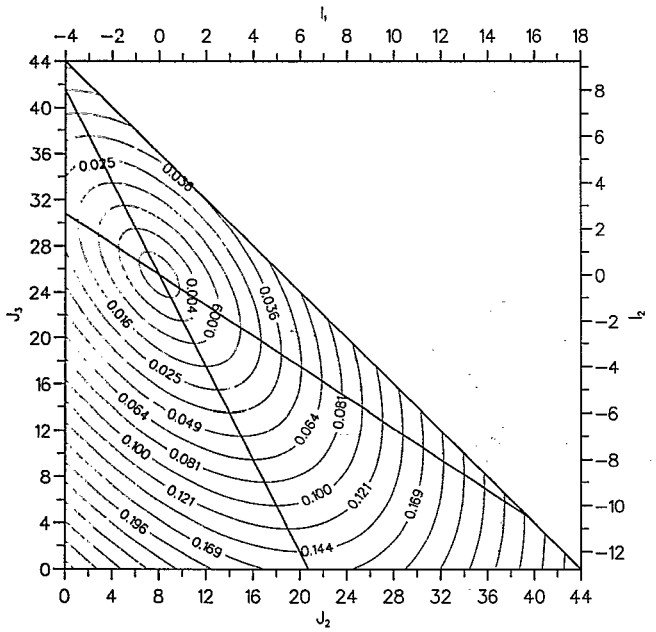

FIG. 3. The zeroth-order energy profile in terms of the two action coordinate systems. The LORC's pertaining to the three-oscillator system are also illustrated. The parameters are $\omega_\alpha = 0.004$, $\omega_\beta = 0.003$, $\omega_{\alpha\beta} = 0.002$, $V_\alpha = 0.003$, and $V_\beta = 0.008$ as also for Figs. 4–7.

which also illustrates the locations of the LORC's and the conversion between (J_2,J_3) and (I_1,I_2); the zero-order energy minimum for the two-pendulum system occurs at $I_1 = 0 = I_2$ (corresponding to $\mathbf{J}^r$), and the high-energy limit is where the resonance zones are well separated.

The two-pendulum system has two degrees of freedom, and so can be studied via Poincaré sections taken at a given total energy. For this work we use the sectioning condition $\psi_2 = \pi$, i.e., pendulum 2 is at the minimum of its potential. If we were to follow the usual sectioning technique, we would plot I_1 and ψ_1 each time the sectioning condition is met with I_2 positive (say) for a trajectory. However, we often find it more revealing to plot the three remaining coordinates I_1, I_2, and ψ_1 as a suitable projection of a three-dimensional space, as illustrated in the figures described below. Regarding the general shape of the sections, note that at low energies, close to the intersection of the LORC's, there is insufficient energy for either pendulum to rotate. In particular, since there is insufficient energy for pendulum 1 [the (I_1,ψ_1) pendulum] to rotate, the section takes the form of a distorted sphere; see, e.g., Fig. 7. At higher energies, where there is sufficient energy for pendulum 1 to rotate, the section takes the form of a distorted tube along the direction parallel to the ψ_1 axis, and is 2π periodic in ψ_1; see, e.g., Figs. 4 and 6. All sections described result from many trajectories (typically ~ 80) propagated at the chosen total-energy value, E.

We consider first the nature of the phase space at relatively high energies, $E \gtrsim 0.06$, well away from the intersection of the LORC's and outside the intersection zone illustrated in Fig. 2. In this energy regime three different types of trajectory occur: trajectories with both pendula rotating corresponding to being outside either resonance zone of Fig. 2, trajectories for which pendulum 1 librates as pendulum 2 rotates correspond to the resonance zone between oscillators 1 and 2, and trajectories for which pendulum 2 librates as pendulum 1 rotates correspond to the resonance zone for oscillators 1 and 3.

The dynamics are almost entirely regular in this energy range. An illustration is given in Fig. 4 which shows a Poincaré section for a constant energy surface $E = 0.07$, from which regions of phase space corresponding to the two resonance zones can be identified. For example, an exact resonance between oscillators 1 and 2 appears as a period-one orbit corresponding to a trajectory in which pendulum 1 executes complete libration each time pendulum 2 rotates ("libration–rotation" in Fig. 4); and quasiperiodic trajectories in which pendulum 1 librates as pendulum 2 rotates—corresponding to the oscillator 1–2 resonance zone— are evident as concentric ellipses about this point. This region is separated from that part of phase space in which both pendula are rotating (i.e., outside either resonance zone) by a clear stochastic layer. Within the layer is found an unstable orbit in which pendulum 1 librates about the maximum of its potential as pendulum 2 rotates. Notice that this stochastic layer appears almost elliptical, the usual shape for stochastic layers about resonance zones.[1]

Similar behavior is evident about a resonance between oscillators 1 and 3. However, due to the sectioning choice, exact resonances between oscillators 1 and 3 appear a period-2 orbits in Fig. 4 (pendulum 2 passes through the section once in each direction during its motion, rotation–libration in Fig. 4). Around such an orbit is a region of phase space in which pendulum 2 librates as pendulum 1 roates. This is delimited by a stochastic layer separating it from regions of phase space in which both pendula are rotating, the layer appearing as "strips" across the Poincaré section. The analogous orbit to the unstable motion described above (where pendulum 1 rotates as 2 librates about is maximum) will not of course appear in the section but has been observed by direct examination.

Although not apparent from Fig. 4, we also find in this

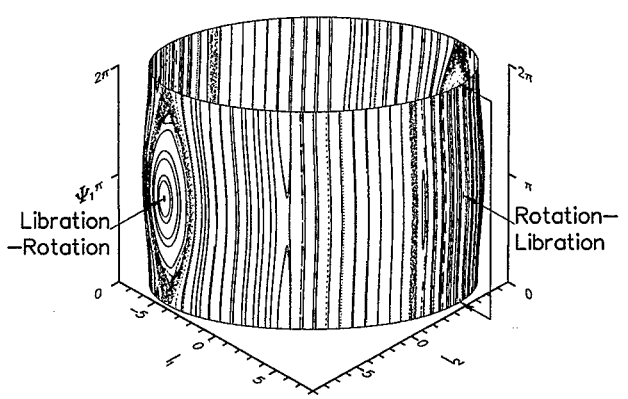

FIG. 4. Poincaré section for the two-pendulum system (sectioning condition $\psi_2 = \pi$) taken at an energy ($E = 0.07$) above that at which it is possible for trajectories to sample the intersection zone. Points resulting from 160 trajectories are shown. The two labels refer to orbits described in the text.

section numerous fixed points and periodic orbits corresponding to trajectories in which both pendula are rotating—either in the same or opposite directions, and either in phase or out or out of phase by π. Obviously, the relative rotation rates of the pendula determine the period of the corresponding orbit in the Poincaré section.

The thickness of the stochastic layers referred to above is found to decrease on moving further away from the resonance intersection zone—that is, increasing further the energy of the two-pendulum system—and it is expected that at arbitrarily high energy they will have vanishingly small thickness. By numerical investigation it is found that the widths of the nonintersecting resonance zones are well predicted by Eq. (3.17) [With V_α and V_β constant as above for the two-pendulum Hamiltonian (4.1)], which implies that the two-pendulum system resonance width are largely independent of energy.

We have seen that it is possible to identify and characterize different regions of the Poincaré section in relation to the resonance zones introduced in Sec. III, and we mentioned there that we would expect the most widespread chaos to be associated with that region of phase space where the resonance zones intersect in the $J_{\text{tot}} = \text{const}$ triangle. To point this up we show in Fig. 5 the location of the LORC's in **I** space, together with the associated resonance widths for the two-pendulum Hamiltonian, obtained from Eq. (3.17). The intersection zone is delimited by the parallelogram $ABA'B'$; at point A, for example, intersection just occurs between an oscillator 1–3 resonance centered on point a and an oscillator 1–2 resonance centered on point b. The kinetic energy of the two-pendulum Hamiltonian (4.1) is

$$E_K(I_1,I_2) = \tfrac{1}{2}\omega_\alpha I_1^2 + \tfrac{1}{2}\omega_\beta I_2^2 + \omega_{\alpha\beta} I_1 I_2,$$

and contours of constant kinetic energy appear in the (I_1,I_2) plane as concentric ellipses, increasing in area as the kinetic energy is increased. Figure 5 also shows a particular contour of constant kinetic energy, $E_K(I_1,I_2) = E_{K,\min}$ ($= 0.049$ with the chosen parameters) such that the contour just touches the intersection zone at the points A and A' described above.

Consider now an arbitrary trajectory at constant total energy E. Since the potential-energy contribution

$$E_P(\psi_1,\psi_2) = V_\alpha \cos\psi_1 + V_\beta \cos\psi_2$$

is bonded above by $E_{P,\max} = E_P(0,0) = V_\alpha + V_\beta$ ($= 0.011$), the kinetic energy is bounded below by $E_K(I_1,I_2) \geqslant E - V_\alpha - V_\beta$. Hence, for $E > E_{K,\min} + V_\alpha + V_\beta = 0.06$, the system is guaranteed not to sample the intersection zone region of the (I_1,I_2) plane illustrated in Fig. 5. This gives an upper estimate of $E = 0.06$ for the energy above which widespread chaos due to intersection of the primary resonances is not expected to occur. To obtain a lower (and probably more accurate) estimate of the energy threshold for widespread chaos, note that since E_P is bounded below by $E_{P,\min} = E_p(\pi,\pi) = -(V_\alpha + V_\beta)$, the kinetic energy is bounded above by $E_K(I_1,I_2) \leqslant E + V_\alpha + V_\beta$. Hence, for $E \leqslant E_{K,\min} - V_\alpha - V_\beta = 0.038$, all trajectories are guaranteed to lie inside the region of the (I_1,I_2) plane bounded by the constant kinetic-energy ellipse

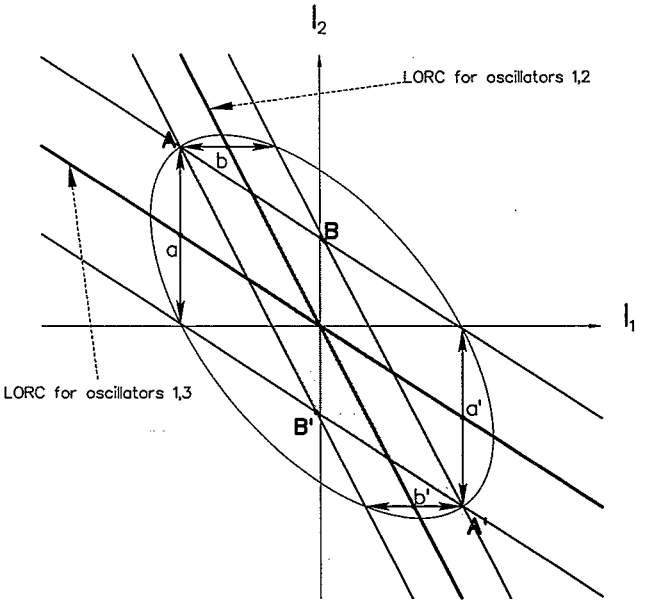

FIG. 5. A schematic illustration of the intersection zone for the two-pendulum system. The points labeled are fully described in the text.

$E_K(I_1,I_2) = E_{K,\min}$, and many such are expected to sample the intersection zone.

The comments above consider chaotic behavior arising solely from intersection of the primary resonances. In reality, of course, an "intersection criterion" neglects stochasticity arising from interaction of rotation–rotation resonances (which can be directly observed), corresponding to motion in which both pendula are rotating and associated with areas of **I** space outside the intersection zone and between the resonance zones, i.e., close to the points A and A' of Fig. 5.

To illustrate the chaos associated with the resonance intersection zone, we show in Fig. 6 two Poincaré sections at $E = 0.015$ [Fig. 6(a)] and at $E = 0.0$ [Fig. 6(b)]. In both cases there is clearly widespread chaos, although there still exist regular regions around particular stable periodic orbits. This is found to be the case generally, but with different stable periodic orbits occurring at different energies. For example, in the $E = 0.015$ case, the significant region of regularity evident in the section is associated with "rotation–rotation" motion in which both pendula are rotating (close to B or B' in Fig. 5); the regular region is not broken up by the appearance of stochastic zones about rotation–rotation resonances and has the effect of dividing the stochastic zones into two parts. In contrast, this regular motion has been destroyed by $E = 0$ [Fig. 6(b)] and the small regular region centered on $I_1 \approx 0 \approx I_2$ and $\psi_1 = \pi$ in this case is due to in-phase normal-mode motion of the two pendula.

As E is decreased further a reversion to wholly regular behavior, connected in part to a growth of the above-mentioned normal-mode motion, is seen in the Poincaré section. The minimum total energy the system may have is $E = -V_\alpha - V_\beta = -0.011$, and for $-0.011 < E \lesssim -0.0055$ the motion appears to be entirely regular, with the Poincaré section taking the form of a distorted sphere as

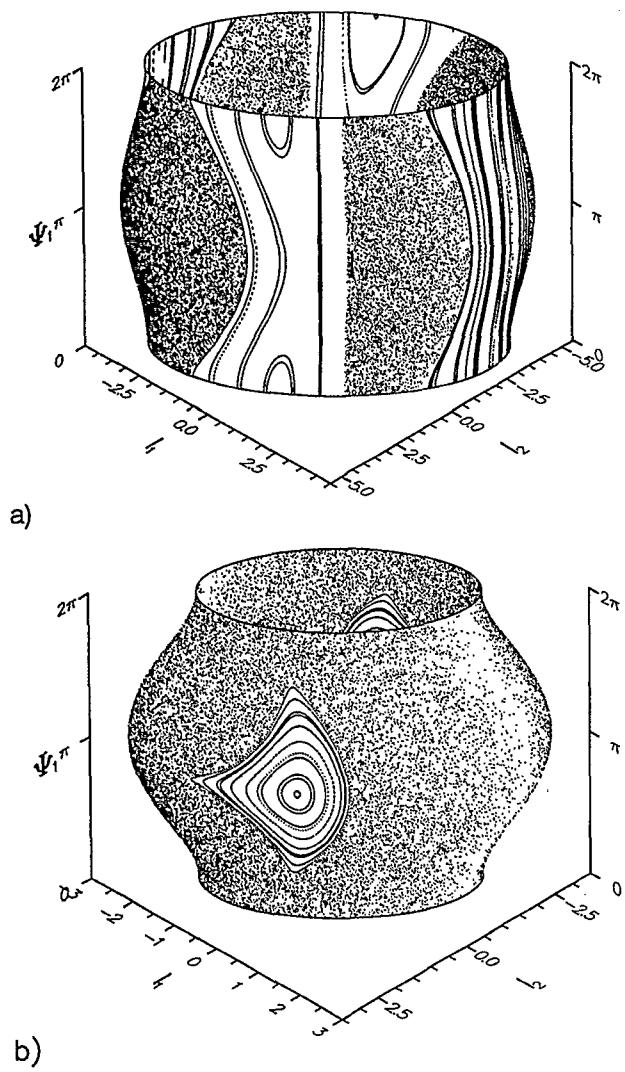

FIG. 6. Poincaré sections for the two-pendulum system (condition $\psi_2 = \pi$) taken at (a) $E = 0.015$ and (b) at $E = 0.0$; i.e., both at energies such that the intersection zone may be sampled. Points resulting from 80 trajectories are illustrated in each case. Widespread chaos is evident in either case.

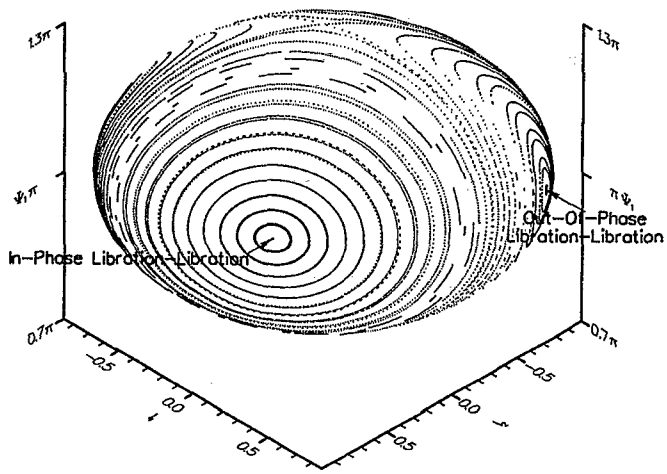

FIG. 7. Poincaré section for the two-pendulum system taken at very low energy ($E = -0.01$) where the dynamics are entirely regular. The labels refer to the two periodic orbits described in the text. Points resulting from 40 trajectories are illustrated in each case.

illustrated in Fig. 7 for $E = -0.01$. The prevalence of regular motion at the lowest energies is not surprising, for the two-pendulum Hamiltonian (4.1) can then be approximated as that for two coupled harmonic oscillators and there naturally appear in the Poincaré section two stable period two orbits corresponding to in-phase and out-of-phase normal mode motions.

We do not fully understand the origins of the first appearance of chaos as E is increased from its minimum value. There is a trivial unstable fixed point of the two-pendulum Hamiltonian (4.1) at $I_1 = 0 = I_2$, $\psi_1 = 0$, $\psi_2 = \pi$ [pendulum 1 (2) stationary at its maximum (minimum)], corresponding to a total energy $E = V_\alpha - V_\beta = -0.005$ and appearing as an unstable fixed point in the Poincaré section, and the first appearance of stochasticity seems to occur at an energy slightly below this. The in-phase normal mode can be followed to energies much higher than those for which a harmonic approximation is reasonable, but it remains stable, with a significant associated regular region, well above the first appearance of stochastic zones [see, e.g., Fig. 6(b)]. We have managed to follow the out-of-phase normal mode only to an energy slightly below that at which stochasticity is first observed. As the energy is increased towards this point, the trajectories are such that the amplitude for librational motion of pendulum one is much greater than that for pendulum two. In fact, as the energy is increased, pendulum two lingers at the minimum of its potential for an increasingly large proportion of its orbit. At a certain energy, it appears that the motion of pendulum two acquires a "kink" each time it is close to this potential minimum (twice in each orbit). This changes the period-two orbit of the Poincaré map into a period-six orbit in a seemingly discontinuous way, and with no apparent change in the stability of the orbit in question. The existence of stochasticity appears to be related to the formation of Poincaré–Birkhoff chains around this remnant of the out-of-phase libration–libration orbit, but this requires further investigation.

V. FIXED POINTS AND PERIODIC ORBITS IN THE TWO-PENDULUM POINCARÉ SECTION

The flow of any two-pendulum trajectory under Hamilton's equations, from one point on the Poincaré section satisfying $\psi_2 = \pi$ to the next, defines a mapping of the remaining coordinates: $I_2, I_1, \psi_1 \to I_2', I_1', \psi_1'$. Given the constraint of constant total energy E, such that I_2 (say) can be eliminated, the mapping is thus two dimensional and area preserving (although with the choice of section it is not necessarily continuous). The sole variable parameter in the mapping is E.

Many examples of single-parameter two-dimensional area-preserving maps have been studied (see, e.g., Refs 16–19), and although the present mapping is significantly different, many of its diverse features are common to previously studied examples. To illustrate this we now describe the behavior of a small representative number of fixed points and periodic orbits in the two-pendulum Poincaré section as the

total energy is increased. Since, for any given E, constant I_1, ψ_1, and ψ_2 ($=\pi$) restricts I_2 to one of two possible values [Eq. (4.1) is quadratic in I_2], we consider (I_1,ψ_1) to be a fixed point of the mapping only if the image point also has the same value of I_2. The location and stability of the fixed points and periodic orbits have been studied by an algorithm due to Child.[20] To determine the stability of an arbitrary fixed point (I_1^0,ψ_1^0) of the Poincaré mapping, we calculate the stability matrix A about his point; that is,

$$A=\left.\frac{\partial(I_1',\psi_1')}{\partial(I_1,\psi_1)}\right|_{(I_1^0,\psi_1^0)},$$

where (I_1',ψ_1') is the image of the point (I_1,ψ_1) under the mapping. Because the mapping is area preserving, the matrix A will have unit determinant and two eigenvalues whose product is unity. If the two eigenvalues are real, i.e., $\lambda_\pm = +e^{\pm\mu}$ or $-e^{\pm\mu}$ then the fixed point is unstable; but if the two eigenvalues are complex, i.e., $\lambda_\pm = e^{\pm i\mu}$, then the fixed point is stable.

A. Libration–libration→rotation–rotation

At the lowest energy the nonlinear Hamiltonian equations of motion for the two-pendulum system can be well approximated by linear equations; and as discussed in Sec. IV, these can be solved in terms of two normal-mode solutions, one of which has the two pendula librating in phase, the other out of phase by π. At the lowest energy the in-phase libration–libration orbit is stable, and appears in the Poincaré section as a period-two orbit. At the lowest energies, the eigenvalues λ_+ and λ_- pertaining to the in-phase normal mode are both initially complex and close to -1; but as the energy is increased, they move around the unit circle (in opposite directions) until, at an energy $E\simeq 0.008$ below the minimum required for both pendula to rotate together ($E=V_\alpha+V_\beta=0.011$), they meet at $\lambda=+1$. At this point the eigenvalues become real and start to move apart along the real axis, one going to $+\infty$ and one to 0 as E tends towards 0.011 from below.

The two-pendulum system will clearly have an unstable fixed point at $E=0.011$ with both pendula stationary and pointing upwards (i.e., $I_1=0=I_2$, $\psi_1=0=\psi_2$). The in-phase libration–libration trajectory tends towards this unstable fixed point as the energy is increased towards $E=0.011$. Although the algorithm for finding periodic orbits breaks down as this point is approached, it is straightforward to examine the extension of the periodic orbit under consideration above the energy of the fixed point of the Hamiltonian. In fact, above $E=0.011$ we find two period-one orbits, located at the continuation of each of the two points of the period-two libration–libration orbit. Each period-one orbit corresponds to a rotation–rotation trajectory [evident in Fig. 6(a)] with both pendula rotating in phase in the same direction, the two period-one orbits being indentical save for a reversal in the direction of motion; and at their birth the orbits are unstable with λ_+ and λ_- tending to ∞ and 0.

We have thus observed the period-two orbit splitting into two period-one orbits, via a divergence in the eigenvalues of the stability matrix. As the total energy is increased the eigenvalues become closer to unity, which appears to be their large E limits.

We add further that although period-doubling bifurcations are not in this case observed as E is increased, we observe an effect similar to the Hamiltonian squeeze effect of Van der Weele *et al.*,[19] in that the existence of higher-order unstable periodic orbits about a stable central periodic orbit has the effect of reducing the size of the stable neighborhood of the central orbit.

B. Evolution of the libration–rotation orbits

At the highest energies, well outside the intersection zone of Fig. 5, trajectories of the two-pendulum system corresponding to a single exact resonance in the three-oscillator system fall into two categories: those in which pendulum 1 librates as pendulum 2 rotates (libration–rotation), corresponding to the oscillator-1–oscillator-2 resonance zone; and those in which pendulum 1 rotates as pendulum 2 librates (rotation–libration), corresponding to the oscillator 1–3 resonance zone. Here we describe evolution with increasing E of the fixed point in the Poincaré map corresponding to libration–rotation about the center of the oscillator 1–2 resonance zone, leading to a period-doubling bifurcation cascade; essentially identical behavior is found for the corresponding rotation–libration orbit.

We have been able to follow the fixed points of the Poincaré map corresponding to the above libration–rotation motion, from its first appearance at an energy, $E\simeq 0.009$ just above that required for pendulum 2 to rotate, up to very high energies ($E\simeq 10$). The fixed point first appears as one of a pair born at the same energy. A discussion of the appearance of a pair of fixed points in terms of normal forms is given in Ref. 21. Here we follow a different approach based on a result of Greene *et al.*[16] that for the two-dimensional area-preserving map derived from a two-degree-of-freedom Hamiltonian, periodic orbits with points on a symmetry line will maintain points on the symmetry line, as will their descendants.

At energies just below that at which the fixed points are born, the image of the symmetry line $\psi_1=\pi$ is found not to cross the symmetry line itself in the region local to where the fixed points are subsequently born (obviously, the existence of other fixed points well away from this may cause such a crossing). At a certain energy, however, the image of the symmetry line will just touch the symmetry line itself. Although not sufficient to prove that a fixed point of the mapping occurs, this condition is necessary, so this is obviously a good place to look for such; and in the present case the point of touching (at $E=0.009$) is indeed a fixed point. As the energy is increased further, the image of the symmetry line moves across the symmetry line, crossing it at two points, both of which are found to be fixed points of the mapping. At the exact birth energy, the eigenvalues of the stability matrix for both fixed points are unity, but as the energy is increased further it becomes apparent that one of the points is stable and the other unstable. As the energy is increased, one of the (real) eigenvalues of the unstable orbit increases rapidly as

the other decreases, until we are no longer able to follow the orbit.

The eigenvalues of the stable periodic orbit (corresponding to the stable fixed point) move around the unit circle of the complex plane as energy is increased, unit they meet at $\lambda_+ = \lambda_- = -1$ for $E = 0.009\,96$, and the orbit becomes unstable. At this stage, it is found that the symmetry line in the vicinity of the fixed point is mapped onto itself, though rotated by π. Increasing the energy further causes the image of the symmetry line to distort into an "S"-shape, crossing the symmetry line at two points other than the fixed point itself. Because the symmetry line is being rotated by $\sim\pi$ as well as being distorted, these auxiliary points cannot be fixed points of the Poincaré mapping P. However, it is possible for them to be fixed points of the mapping P^2, which in this case they are. The stable period two orbit (of P) so produced has stability matrix eigenvalues equal to unity at its birth. (This is the expected result, for the stability matrix of P^2 will be A^2 when the period-two orbit is first born, and so will have eigenvalues λ^2_+ and λ^2_-. As $\lambda_+ = \lambda_- = -1$ the eigenvalues of A^2 will be $+1$).

This period-doubling bifurcation is repeated when the eigenvalues of the stability matrix for the period-two orbit have moved around the unit circle to -1, producing a period-four orbit. This period-four orbit is found to bifurcate to a period-eight one, which in turn bifurcates to one of period 16. This is as far as we have been able to follow the bifurcation cascade numerically, but it is expected to continue *ad infinitum*. We are naturally unable to test this mapping for universality but we do note that the pattern produced in the Poincaré section by the higher-order periodic orbits, in all cases of such sequences obtained in the two-pendulum system, is very similar to that observed by Bialek, Schmidt, and Wang for a bifurcation sequence pertaining to a particle in a standing wave field (Fig. 3 of Ref. 22) and by Greene *et al.* for a period-doubling sequence of the DeVogelaere quadratic map (Fig. 3 of Ref. 19).

After the period-doubling sequence, the period-one fixed point is unstable for a significant energy range (from $E = 0.009\,96$ to $E = 0.0155$). For the lower part of this energy range, we were able to follow the higher-order orbits, and for none of these (other than the root period-one orbit) was evidence found that they returned to stability. As far as was numerically feasible to follow them, in all cases the eigenvalues of the stability matrix moved apart along the negative real axis. The period-one fixed point did return to stability with increasing E at $E = 0.0155$, but no period-doubling sequence was observed as E was decreased through this value. As the energy is increased further into the region where the period-one orbit is again stable, the eigenvalues of the corresponding stability matrix move around the unit circle and, in the limit of very high energy tend towards unity.

Numerous other fixed points and periodic orbits have been followed over a wide energy range,[23] and many period-doubling bifurcation sequences have been observed. We were not able to follow any of these sequences sufficiently to establish whether or not the system obeys universality, but in all cases the pattern made by the higher-order orbits in the section was as described above. There is no apparent global pattern to the evolution of fixed points and periodic orbits: although the above rotation–libration and libration–rotation orbits seemed to follow the same pattern from low to high energies, there exist in addition many orbits which do not follow such a simple pattern, possibly alternating between stability and instability several times as energy is varied.

VI. THE THREE-OSCILLATOR SYSTEM

To examine the extent to which the behavior of the three-oscillator model is adequately described by the resonance Hamiltonian (3.11), or the corresponding two-pendulum Hamiltonian (4.1), we have studied the classical dynamics of the full three-oscillator system. A brief account of this is now given.

Instead of propagating trajectories directly in $(\mathbf{J},\boldsymbol{\theta})$ space or $(\mathbf{I},\boldsymbol{\psi})$ space, we have chosen to propagate Hamilton's equations in $(\mathbf{p},\mathbf{q})$ space. The reason for this is purely computational: conversion between the coordinate systems is certainly required for the initial conditions (and often along the trajectory itself), but the computer is not forced to determine a large number of sine and/or cosine terms, thereby reducing the expense of the calculation. By propagating the six equations of motion for the three-oscillator system using variable-order variable-step Adams integrator routines supplied by the Numerical Algorithms Group, it was possible to conserve energy to better than one part in 10^{14}.

Poincaré sections are a less appropriate tool for ascertaining the regular or stochastic nature of trajectories in the three-degree-of-freedom system. For such an assignment to be made two sectioning conditions must be imposed, but the probability of two such conditions being simultaneously satisfied along a particular trajectory is vanishingly small. One of the conditions must therefore by relaxed (say record the other coordinates of the trajectory whenever $p_1 = 0$, $|p_2| < \delta$), but this leads to "fuzziness" on the section and so limits the accuracy of any assignments. Even with such a relaxation of sectioning conditions, Poincaré sectioning is almost prohibitively expensive for the three-degree-of-freedom system. Further, it is capable only of revealing the existence or otherwise of a third integral of the motion: in the absence of a third integral of the motion, no information can be gleaned about the second (conservation of energy dictates at least one integral of the motion).

The use of power spectra in characterizing classical trajectories has also been widely considered (see, e.g., Ref. 24). If the power spectrum of a single trajectory is regular (i.e., it consists of a few narrow peaks), then the trajectory itself is regular. However, a "grassy" power spectrum frequently cannot be unambiguously assigned: it may arise either from a chaotic trajectory or from a quasiperiodic one with many underlying frequencies. This limits somewhat the usefulness of power spectra as a diagnostic tool.

Although we have studied both Poincaré sections and power spectra,[23] we have found Lyapunov exponents (see, e.g., Ref. 25) to be the most useful diagnostic in characterizing trajectories of the three-oscillator model. By direct measurement of the rate of exponential divergence of adjacent

trajectories, we are able to establish the number of integrals of the motion for particular trajectories at considerably less computational expense (a few hours CPU time on a SUN 4/370 workstation being required for each trajectory). A fully comprehensive study of the six-dimensional phase space is clearly not feasible, and we have principally studied regions associated with the resonance and intersection zones of the resonance and two-pendulum Hamiltonians. The results summarized briefly below follow by analysis of the Lyapunov exponents for numerous trajectories of the three-oscillator system, supported where appropriate by consideration of power spectra and Poincaré sections.

VII. RESULTS

In reducing the three-oscillator Hamiltonian to the resonance Hamiltonian (3.11), all fast-moving angle terms were neglected. This resonance approximation had the effect of making I_3 a constant of the motion, and thus $J_{\text{tot}} \equiv 2J_1 + J_2 + J_3$ was constant for any trajectory. It is straightforward to examine the validity of this approximation by directly propagating trajectories and thereby calculating J_{tot} as a function of time. To facilitate comparison with the two-pendulum work, and with corresponding quantum-mechanical studies to be described in a forthcoming publication,[13] we restrict our study of trajectories for the three-oscillator system to the case of $J_{\text{tot}}(t=0) = 44$. For all trajectories it was found that the variation in J_{tot} was less than 0.1. Although larger than numerical error (and thus a "real" effect), this variation is much less than typical variation ($\sim$1–10) in any of the individual J_i's, and as expected is of very high frequency, being related to fast-moving terms in the three-oscillator Hamiltonian. The resonance approximation thus appears to be a good one.

The locations and widths of the resonance zones associated with the resonance Hamiltonian (3.11) are estimated from Eqs. (3.15) and (3.17), and these appear to predict well the extent of the resonance zones in the three-oscillator system. Trajectories initiated in regions of the full six-dimensional phase space corresponding to a single resonance zone in the resonance Hamiltonian are found capable of exploring regions of action space up to the full width predicted by Eq. (3.17). Naturally (as for the two-pendulum system), not all trajectories initiated within a resonance zone explore its full width. This is illustrated in Figs. 8(a) and 8(b), which show [as a projection onto the (J_2,J_3) plane] the regions of **J** space explored by two trajectories of the three-oscillator system initiated inside the oscillator-1–oscillator-2 resonance zone. In Fig. 8(a) the system was initiated close to the center of the resonance (corresponding in the two-pendulum system to low-amplitude librational motion for pendulum 1), and samples only a small fraction of the full width. In Fig. 8(b), however, the system was initiated close to the edge of the resonance zone (corresponding to high-amplitude librational motion for pendulum 1), and is able to explore essentially the full width of the resonance.

The J_3 dependence of the resonance zone width for the oscillator-1–oscillator-2 resonance (and similarly the J_2 dependence of that pertaining to the oscillator-1–oscillator-3 resonance) is also found to be well estimated by Eq. (3.7) appropriate to the resonance Hamiltonian. Although the two-pendulum Hamiltonian (4.1) [with $V_\alpha \equiv V(\{J_i^r\})$ and $V_\beta(\{J_i^r\})$ constant] is not constructed to address this dependence, it is evident from Fig. 2 that even this gives a reasonable estimate of the resonance widths.

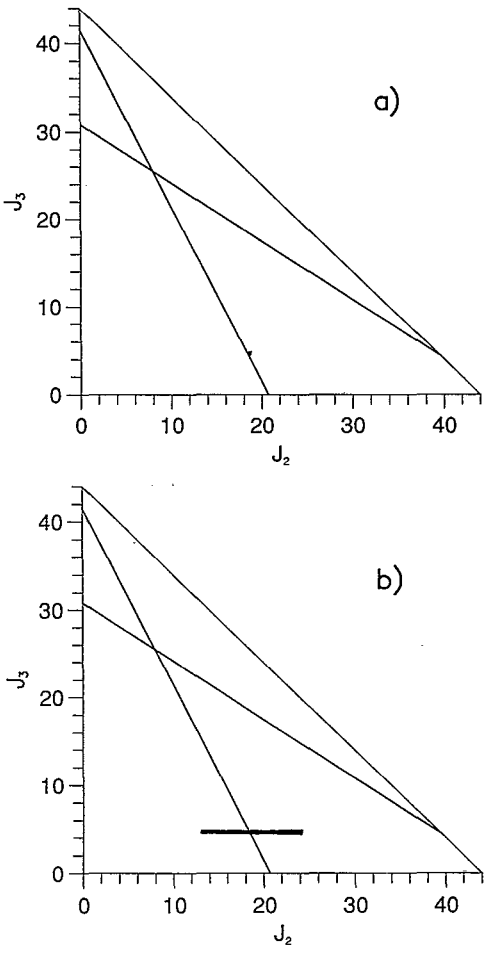

FIG. 8. Representative trajectories for the full three-degree-of-freedom system projected onto the (J_2,J_3) plane. Both trajectories are initiated inside the oscillator 1–2 resonance zone of Fig. 2 (but outside the intersection zone). Identical values of $J_3(t=0)$ are taken in either case but in (a) the trajectory is initiated close to the LORC, whereas in (b) the trajectory is initiated close to the edge of the resonance zone and samples the full width.

The above comments are pertinent to total energies such that the resonance intersection zone is not sampled by trajectories. The result of Sec. IV for the two-pendulum Hamiltonian would suggest that stochasticity in this energy domain should be associated with the borders of the resonance zones, and that the thickness of the resultant "stochastic tubes" in the full six-dimensional phase space (as opposed to stochastic layers in the two-pendulum system) should generally diminish on moving further away from the intersection zone. From the regions of phase space we have probed, it appears that such a picture is appropriate. This can be addressed by examination of the Lyapunov exponents for a range of trajectories with different angles, close to the edges of a particu-

lar resonance zone, and moving progressively along the edge of that resonance zone further away from the intersection zone. The thickness of the walls of the stochastic tubes is indeed found to decrease the further away one moves from the intersection zone, although the stochastic regions are somewhat larger than those for the corresponding two-pendulum system, as the latter neglects fast-moving terms and the variation of V_α and V_β along any trajectory.

Commensurate with the predictions of the two-pendulum system, the most widespread chaos in the full three-oscillator system occurs in the intersection zone region: a very large fraction of trajectories initiated in this region have at least one pair of nonzero Lyapunov exponents. The volume of action space sampled by trajectories initiated inside the intersection zone is also typically far greater than those initiated outside it. This is illustrated in Fig. 9 which shows [again as a projection onto the (J_2,J_3) plane] the **J**-space regions sampled by a representative trajectory initiated well inside the intersection zone. As can be seen from the figure, much of the intersection zone is sampled, motion in the direction of both J_2 and J_3 being facile for such trajectories.

As also predicted from the two-pendulum model, there naturally exists in the three-oscillator system a small regular region towards the center of the intersection zone. Trajectories initiated in this region correspond to the low-amplitude libration–libration motion of the pendula, are regular, and do not explore much of the action space.

Regular regions around certain stable periodic orbits were observed in the two-pendulum system even in an energy domain where most of phase space was stochastic, see, e.g., Fig. 6. Corresponding behavior in the three-oscillator system was not observed: the perturbing influence of the fast-moving terms, and the variation of V_α/V_β with $\{J_i\}$, increases the stochastic volume and appears to squeeze such regular regions out of existence.

In addition to chaotic behavior as a result of intersecting resonances, another chaotic phenomenon associated with higher-dimensional Hamiltonian systems is that of Arnol'd diffusion. This process may occur in systems with three or more degrees of freedom, where the KAM tori formed by quasiperiodic trajectories are unable to divide phase space. Our three-oscillator system has two resonances, and it is expected that any consequent Arnol'd diffusion outside the intersection zone would be manifest as motion along the length of the "stochastic tubes" around the individual resonance zones. The ergodicity thus far described in this region has been the result of motion *around* these stochastic tubes and *across* the stochastic volume. A commonly invoked model for Arnol'd diffusion[26] involves three resonances: one acting as a guide, the second being responsible for the formation of a stochastic volume around the guide, and the third resonance inducing motion along the stochastic volume. In our three-oscillator model there exist in addition to the two main resonances, Fourier terms that will drive motion out of the constant $J_{\rm tot}$ plane [the "fast-moving" angle terms in Eq. (3.10)]. In employing the resonance approximation, these terms are "averaged over" and thus neglected. Although they do not constitute a third resonance, is it possible for these terms to induce Arnol'd diffusion? Because the resonance approximation gives a very good caricature of the three-ocillator system, we would expect any effect from such neglected terms to be small, and indeed we did not find evidence of any kind for the existence of Arnol'd diffusion. Many trajectories were initiated in the stochastic tubes around the resonance zones (though away from the intersection zone), and the mean-square displacement from the starting condition up to time t,

$$\langle \Delta J^2 \rangle = \frac{1}{N} \sum_{n=1}^{N} |\mathbf{J}(t_n) - \mathbf{J}(0)|^2,$$

was calculated for each. In all cases it was found that this quantity approached a finite limit corresponding to the mean-square displacement from the initial conditions around the "tube." There was no long-term increase in this quantity which would be expected if there was any motion along the length of the tube, a result confirmed by a direct examination of the coordinates along any trajectory.

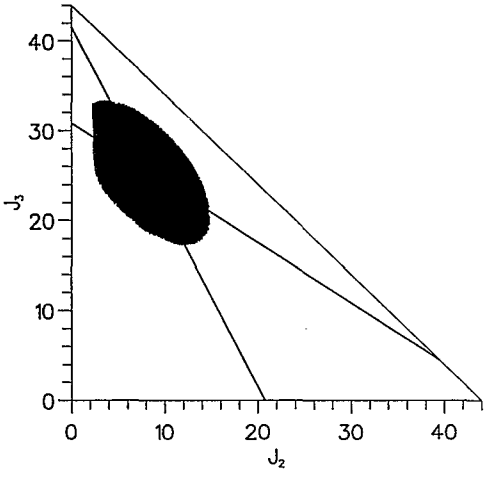

FIG. 9. A representative trajectory for the full three-degree-of-freedom system initiated inside the intersection zone, illustrating the widespread ergodicity associated with this region.

ACKNOWLEDGMENTS

We are grateful to M. S. Child, P. G. Wolynes, and M. D. Winn for helpful discussions. K.M.A. is grateful for the award of an SERC studentship.

APPENDIX: THE CHANGE OF PARAMETERS IN THE TWO-DEGREE-OF-FREEDOM HAMILTONIAN

The two-degree-of-freedom Hamiltonian of Sec. IV is [Eq. (4.1)]:

$$H = \tfrac{1}{2}\omega_\alpha I_1^2 + \tfrac{1}{2}\omega_\beta I_2^2 + \tfrac{1}{2}\omega_{\alpha\beta} I_1 I_2 + V_\alpha \cos\psi_1 + V_\beta \cos\psi_2. \tag{A1}$$

For positive ω_α, ω_β, and $\omega_{\alpha\beta}$, this is a Hamiltonian for two-coupled pendula, where the terms involving I_1 and I_2 play the role of kinetic energy and the V terms correspond to potential energy. However, the resonance approximation to the three-oscillator Hamiltonian with negative parameters

$\{\hat{\omega}_i\}$ results in negative values for the ω_α, ω_β, and $\omega_{\alpha\beta}$. Here we trivially transform the resultant Hamiltonian into one in which the kinetic-energy terms are positive, and which displays *identical* dynamical behavior to that generated by Eq. (A1) with $\{\omega_\alpha,\omega_\beta,\omega_{\alpha\beta},V_\alpha,V_\beta\}<0$. The above Hamiltonian gives (via Hamilton's equations) the following equations of motion for the coordinates $\mathbf{I}$ and ψ:

$$\frac{d\psi_1}{dt}=\frac{\partial H}{\partial I_1}=\omega_\alpha I_1+\omega_{\alpha\beta}I_2, \tag{A2a}$$

$$\frac{d\psi_2}{dt}=\frac{\partial H}{\partial I_2}=\omega_{\alpha\beta}I_1+\omega_\beta I_2, \tag{A2b}$$

$$\frac{dI_1}{dt}=-\frac{\partial H}{\partial \psi_1}=V_\alpha \sin\psi_1, \tag{A2c}$$

$$\frac{dI_2}{dt}=-\frac{\partial H}{\partial \psi_2}=V_\beta \sin\psi_2. \tag{A2d}$$

We make the (obviously noncanonical) transformations

$$\begin{aligned} &I_1'=-I_1,\quad I_2'=-I_2,\\ &\psi_1'=\psi_1,\quad \psi_2'=\psi_2,\\ &\omega_\alpha'=-\omega_\alpha,\quad \omega_\beta'=-\omega_\beta,\quad \omega_{\alpha\beta}'=-\omega_{\alpha\beta},\\ &V_\alpha'=-V_\alpha,\quad V_\beta'=-V_\beta, \end{aligned} \tag{A3}$$

and use Eq. (A2) to predict the time-dependent behavior of the new coordinates. It is possible to find a new Hamiltonian, $H'=H'(I_1',I_2',\psi_1',\psi_2')$, as a function of these new coordinates and parameters, whose equations of motion are identical to those for I_1, I_2, ψ_1, and ψ_2 deduced from Eqs. (A2) and (A3) appropriate to H. Thus, we have from Eqs. (A2) and (A3)

$$\begin{aligned} &\frac{d\psi_1'}{dt}=\frac{d\psi_1}{dt}=\omega_\alpha I_1+\omega_{\alpha\beta}I_2=\omega_\alpha' I_1'+\omega_{\alpha\beta}' I_2'=\frac{\partial H'}{\partial I_1'},\\ &\frac{d\psi_2'}{dt}=\frac{d\psi_2}{dt}=\omega_{\alpha\beta} I_1+\omega_\beta I_2=\omega_\alpha' I_1'+\omega_{\alpha\beta}' I_2'=\frac{\partial H'}{\partial I_1'},\\ &\frac{dI_1'}{dt}=-\frac{dI_1}{dt}=-V_\alpha \sin\psi_1=V_\alpha' \sin\psi_1'=-\frac{\partial H'}{\partial \psi_1'},\\ &\frac{dI_2'}{dt}=-\frac{dI_2}{dt}=-V_\beta \sin\psi_2=V_\beta' \sin\psi_2'=-\frac{\partial H'}{\partial \psi_2'}, \end{aligned} \tag{A4}$$

Now, we can integrate up Eqs. (A4) to get the new Hamiltonian, H', in terms of the new coordinates. Neglecting the arbitrary constant, this gives

$$\begin{aligned} H'=&\tfrac{1}{2}\omega_\alpha' I_1'^2+\tfrac{1}{2}\omega_\beta' I_2'^2+\omega_{\alpha\beta}' I_1' I_2'\\ &+V_\alpha' \cos\psi_1'+V_\beta' \cos\psi_2'. \end{aligned} \tag{A5}$$

This Hamiltonian is essentially identical to that of Eq. (A1) except that all parameters are now positive, and in particular the kinetic-energy term for each pendulum is positive. This means that trajectories resulting from it can be understood in terms of two coupled pendula.

It is important to note that H' is constructed such that its equations of motion in terms of $\mathbf{I}'$ and ψ' are identical to those for H in terms of $\mathbf{I}$ and ψ, with Eq. (A3) prescribing the relation between $(\mathbf{I}',\psi')$ and $(\mathbf{I},\psi)$. This forces the dynamics of the new coordinates to be the same as the dynamics of the old. The flow from the Hamiltonian of Eq. (A4) will mirror exactly the flow from the Hamiltonian of Eq. (A1). (We thus neglect the prime notation in Secs. IV and V.)

[1] B. V. Chirikov, Phys. Rep. **52**, 263 (1979).
[2] D. W. Noid, M. L. Koszykowski, and R. A. Marcus, Annu. Rev. Phys. Chem. **32**, 267 (1981).
[3] S. A. Rice, Adv. Chem. Phys. **47**, 117 (1981).
[4] E. B. Stechel and E. J. Heller, Annu. Rev. Phys. Chem. **35**, 563 (1984).
[5] B. Eckhardt, Phys. Rep. **163**, 205 (1988).
[6] P. V. Elyutin, Sov. Phys. Usp. **31**, 597 (1988).
[7] M. J. Davis, J. Phys. Chem. **92**, 3124 (1988).
[8] P. Brumer and M. Shapiro, Adv. Chem. Phys. **70**, 365 (1988).
[9] A complete list of references relevant to this topic is beyond the scope of this work but would include the following: D. W. Oxtoby and S. A. Rice, J. Chem. Phys. **65**, 1676 (1976); C. Jaffe and P. Brumer, *ibid.* **73**, 5646 (1980); J. S. Hutchinson, W. P. Reinhardt, and J. T. Hynes, *ibid.* **79**, 4247 (1983); E. J. Heller, E. B. Stechel, and M. J. Davis, *ibid.* **73**, 4720 (1980); K. G. Kay, *ibid.* **72**, 5955 (1980); M. J. Davis and S. K. Gray, *ibid.* **84**, 5389 (1986); T. Uzer, Phys. Rep. **199**, 73 (1991); S. C. Farantos and J. Tennyson, J. Chem. Phys. **82**, 800 (1985); R. A. Marcus, Ann. N.Y. Acad. Sci. **357**, 169 (1980); C. C. Martens and G. S. Ezra, J. Chem. Phys. **86**, 279 (1986).
[10] A. A. Stuchebrukhov, M. V. Kuzmin, V. N. Bagratashvili, and V. S. Letokhov, Chem. Phys. **107**, 429 (1986).
[11] D. E. Logan and P. G. Wolynes, J. Chem. Phys. **93**, 4994 (1990).
[12] V. N. Bagratashvili, V. S. Letokhov, A. A. Makarov, and E. A. Ryabov, *Multiple Photon Infrared Laser Photophysics and Photochemistry* (Harwood Academic, Chur, 1985).
[13] K. M. Atkins and D. E. Logan (unpublished).
[14] K. M. Atkins and D. E. Logan, Phys. Lett. A **162**, 255 (1992).
[15] M. Tabor, *Chaos and Integrability in Non-Linear Dynamics* (Wiley, New York, 1989).
[16] J. M. Greene, R. S. McKay, F. Vivaldi, and M. J. Feigenbaum, Physica D **3**, 468 (1981).
[17] T. C. Bountis, Physica D **3**, 577 (1981).
[18] G. Contopoulos, Physica D **8**, 142 (1983).
[19] J. P. Van der Weele, H. W. Capel, T. P. Valkering, and T. Post, Physica A **147**, 499 (1988).
[20] M. S. Child, *Semiclassical Mechanics with Molecular Applications* (Oxford Science, Oxford, 1991).
[21] J. D. Crawford, Rev. Mod. Phys. **63**, 991 (1991).
[22] J. Bialek, G. Schmidt, and B. H. Wang, Physica D **14**, 265 (1985).
[23] K. M. Atkins, D. Phil. thesis, Oxford University, 1991 (unpublished).
[24] R. S. Dumont and P. Brumer, J. Chem. Phys. **88**, 1481 (1988).
[25] H. D. Meyer, J. Chem. Phys. **84**, 3147 (1986).
[26] A. J. Lichtenberg and M. A. Lieberman, *Regular and Stochastic Motion*, edited by F. John, J. E. Marsden, and L. Sirovich, Vol. 38 in Applied Mathematical Sciences (Springer-Verlag, Berlin, 1983).